View metadata, citation and similar papers at core.ac.uk

brought to you by CORE

provided by Online Research Database In Technology

DTU Library

High-Q 3D Microfabricated Magnetic-core Toroidal Inductors for Power Supplies in Package

Thanh Le, Hoa; Nour, Yasser; Pavlovic, Zoran; O'Mathuna, Cian; Knott, Arnold; Jensen, Flemming; Han, Anpan; Kulkarni, Santosh; Ouyang, Ziwei

Published in:
I E E E Transactions on Power Electronics

Link to article, DOI:
10.1109/TPEL.2018.2847439

Publication date:
2018

Document Version
Peer reviewed version

Link back to DTU Orbit

Citation (APA):
Thanh Le, H., Nour, Y., Pavlovic, Z., O'Mathuna, C., Knott, A., Jensen, F., ... Ouyang, Z. (2018). High-Q 3D Microfabricated Magnetic-core Toroidal Inductors for Power Supplies in Package. *I E E E Transactions on Power Electronics*, *34*(1), 74-85. https://doi.org/10.1109/TPEL.2018.2847439

General rights
Copyright and moral rights for the publications made accessible in the public portal are retained by the authors and/or other copyright owners and it is a condition of accessing publications that users recognise and abide by the legal requirements associated with these rights.

- Users may download and print one copy of any publication from the public portal for the purpose of private study or research.
- You may not further distribute the material or use it for any profit-making activity or commercial gain
- You may freely distribute the URL identifying the publication in the public portal

If you believe that this document breaches copyright please contact us providing details, and we will remove access to the work immediately and investigate your claim.

This article has been accepted for publication in a future issue of this journal, but has not been fully edited. Content may change prior to final publication. Citation information: DOI 10.1109/TPEL.2018.2847439, IEEE Transactions on Power Electronics

High-Q 3D Microfabricated Magnetic-core Toroidal Inductors for Power Supplies in Package

Hoa Thanh Le, *Student Member, IEEE*, Yasser Nour, *Member, IEEE*, Zoran Pavlovic, *Member, IEEE*, Cian O Mathuna, *Fellow, IEEE*, Arnold Knott, *Member, IEEE*, Flemming Jensen, Anpan Han, *Member, IEEE,* Santosh Kulkarni, *Member, IEEE*, Ziwei Ouyang, Senior *Member, IEEE**

Abstract— **Integration of power inductors is a roadblock in realizing highly miniaturized power supply in package (PSiP) and power supply on chip (PwrSoC). Inductors in such power system are used for energy storage and filtering, but they dominate in size and loss. This paper presents a novel 3D in-silicon through-silicon via (TSV) magnetic-core toroidal inductor for PSiP. The magnetic powder based core is embedded into TSV air-core inductor using a casting method. The unique air-core inductor design with a hollow core and suspended windings enable a complete core filling with microscale magnetic powders. The proposed casting method is simple, scalable, and generic for a wide range of magnetic powders. TSV magnetic-core inductors are fabricated in a compact size of 2.4 x 2.4 x 0.28 mm with the core content varying from 63 to 88 weight percent of soft ferrite NiZn powders. The TSV magnetic-core toroidal inductors are fabricated and electrically characterized. Small-signal measurements show a three-fold higher inductance of 112 nH and a 30% higher quality factor of 14.3 at 12.5 MHz for magnetic core inductors compared to similar TSV air-core inductors. The small-signal measurement results are verified by the modelled results. The total core loss is characterized by large-signal measurements. A suitable inductor is implemented in a 12-MHz buck converter that operates in a zero-voltage-switching mode. The converter achieves a peak efficiency of 71.6 % and the output power of 2.4 W converting 12 to 5 V_{DC}.**

Index Terms— **Microfabrication, inductor, through-silicon vias (TSV), magnetic materials, PSiP**

This project is a part of TinyPower project which is funded by Innovation Fund (No. 67-2014-1). The authors would like to acknowledge funding from Science Foundation Ireland through their Starting Investigator (15/SIRG/3569) and Investigators Programme (15/IA/3180).

Hoa Thanh Le is with National Center for Micro- and Nanofabrication (DTU Danchip) and DTU Electrical Engineering (DTU Electro), Technical University of Denmark (DTU), 2800 Kongens Lyngby, Denmark. (email: hoalet@nanotech.dtu.dk)

Anpan Han and Flemming Jensen are with DTU Danchip (email: anph@dtu.dk, fj@danchip.dtu.dk)

Cian O Mathuna and Zoran Pavlovic (corresponding author) are with the Microsystems Centre, Tyndall National Institute, University College Cork, Cork, Ireland (email: cian.omathuna@tyndall.ie; zoran.pavlovic@tyndall.ie)

Santosh Kulkarni is with Dialog Semiconductor, Swindon, United Kingdom (Santosh.Kulkarni@diasemi.com)

Yasser Nour, Arnold Knott, and Ziwei Ouyang (corresponding author) are with DTU Electro (e-mail: ynour@elektro.dtu.dk, akn@elektro.dtu.dk, zo@elektro.dtu.dk)

I. Introduction

Miniaturization of power supplies are essential for the development of smart electronics systems e.g. internet of things (IoTs), light emitting diode (LED) lightings, and consumer electronic products [1]–[3]. As more functions are packed in a limited space in such electronic systems, power supplies are required to be more compact and efficient with a lower manufacture cost [4]–[6]. Monolithic integration of power supply has been widely investigated as an ideal solution for miniaturization. The ultimate integrated power supply is power supply on chip (PwrSoC) [5]–[10], in which all active and passive components are integrated on the same die. A shorter-term integration solution is the power supply in package (PSiP) [5], [6] in which the discrete inductors and capacitors are packaged together with the power management integrated circuits. In such power supplies, passive inductors often dominate in size and loss [4]–[6], therefore, reducing inductor's size is essential for PwrSoC development. Because switching at higher frequency enables the use of smaller inductors, the evolution of integrated power supply is highly correlated to the increase in the switching frequency i.e. 10 – 20 MHz for co-packaged or stacked PSiP and to the very high frequency range (30 – 300 MHz) for PwrSoC [9].

Microelectromechanical system (MEMS) technologies have shown a great potential for making compact, high-performance integrated inductors for a wide range of operation frequencies from a few MHz to the VHF range [8], [9]. The important advantage of MEMS inductors over the traditional discrete inductors is the possibility for IC integration and miniaturization. Previous studies investigated on winding structure optimization, magnetic material technology, and fabrication technology to achieve high inductance density, high quality factor (Q), high operation frequency, and low electromagnetic interference (EMI).

Three-dimensional (3D) toroidal inductors [11]–[14] are known for low EMI due to the high flux confinement, high Q, and high operation frequency [15]. Other 2D inductor geometries, for example spiral inductors [16], [17], racetrack inductors [18], [19], and 3D solenoid inductors [20]–[22], have strong out-of-plane stray fields. 3D toroidal inductors are classified into on-silicon (on-Si) toroidal inductors [11], [23]

0885-8993 (c) 2018 IEEE. Personal use is permitted, but republication/redistribution requires IEEE permission. See http://www.ieee.org/publications_standards/publications/rights/index.html for more information.

This article has been accepted for publication in a future issue of this journal, but has not been fully edited. Content may change prior to final publication. Citation information: DOI 10.1109/TPEL.2018.2847439, IEEE Transactions on Power Electronics

and in-silicon (in-Si) toroidal inductors [14], [24]–[26] according to the fabrication technology. Because fabricating in-Si inductors requires bulk micromachining as the windings are constructed in the substrate, in-Si inductor technology is more challenging and often more complex compared to on-Si inductor technology. However, in-Si inductors have some key advantages over on-Si inductors, such as a higher inductance density due to a lower inductor profile and the potential for advanced packaging of PSiP and PwrSoC. With the in-Si winding structures, inductor profile is substantially lower compared to similar on-Si structures. This is an important advantage for IC implementation in some applications where a low power supply profile is crucial, such as mobile phone or wearable applications [27]. Furthermore, in-Si inductors are often involved through-silicon vias (TSV) as part of the windings, therefore, inductor substrate can be used as a passive interposer for co-packaged or stacked PSiP packaging. This approach has been demonstrated by Li et al. [28] with a DC-DC buck PSiP using 2D TSV spiral inductor sandwiched between two magnetic sheets. This approach is a promising packaging technology for PSiP and PwrSoC as power supply footprint can be significantly reduced using TSV-based interposer.

Developing integrated inductors for PSiP often involves magnetic materials to achieve a useful inductance to operate at high-frequency range (10 - 20 MHz) [29]. Integration of the magnetic-core for the toroidal inductors is very challenging [26], [30]. Previous studies have reported on several deposition methods including electrodeposition, sputtering, and screen-printing, each of which has its own advantages and disadvantages as reviewed in [9]. Screen printing is a well-established and comparatively cheap technology that has been adopted for magnetic-core microinductors in the 1990s [31], [32]. The screen printing technique has the advantages of being a rather simple process with a wide range of printable materials, for example NiFe, NiFeCo for the KHz range, MnZn for frequencies below 5 MHz, and NiZn for an operating frequency as high as 10 MHz and above [28], [33]. NiZn is a preference due to its high resistivity and suitable relative permeability.

In this paper, we report a high-Q 3D TSV in-Si magnetic-core MEMS toroidal inductors for high frequency (10 – 20 MHz) power conversions. The specific contributions of this paper include: (i) A simple casting fabrication process for 3D TSV in-Si magnetic-core toroidal inductor integration. The process is demonstrated with, but not limited to, a composite material consisting of a non-conducting polydimethylsiloxane (PDMS) and 17-μm-diameter NiZn powders. The magnetic composite material is embedded into the pre-fabricated MEMS Through Silicon Vias (TSV) air-core toroidal inductors reported in our previous work [34]. The process is also demonstrated with 50-μm-diameter soft magnetic composite (SMC) particles. Furthermore, the reported process is fully compatible with the screen-printing technique for production scaling. (ii) An improved inductor performance in terms of inductance density and quality factor, i.e. 3 times higher inductance and 30% higher quality factor, compared to the prior microfabricated toroidal inductors. (iii) The fabricated inductors are modelled and fully characterized by small-signal measurement, large-signal measurement, and testing in power converter.

This paper is organized as follows: Section II presents the fabrication of the TSV magnetic-core toroidal inductor using a casting process based on a molding approach for a controlled core thickness and void-free magnetic core. Section III presents the magnetic characterization of the magnetic-core material and electrical characterization of the fabricated TSV inductors. The measurement results are compared to the modelled results. Section IV describes the implementation of a 12-MHz buck converter using a TSV magnetic-core toroidal inductor and GaN FETs. The last section concludes the paper.

II. TSV Magnetic-core Toroidal Inductor

For the operational frequencies from 10 to 20 MHz, an inductance of 100s of *nH* is needed to achieve higher power converter efficiency and density. Magnetic core based inductors achieve significantly higher inductance densities in comparison to their air core equivalents, resulting in lower ripple current in the converter and lower losses. Fig. 1 shows the proposed TSV magnetic-core toroidal inductor fabricated based-on a pre-made TSV air-core inductor using a simple casting and curing process for the subsequent filling of the magnetic composite. The dimensions of the 3D TSV air-core toroidal inductor are illustrated in Fig. 1a and presented in Table I.

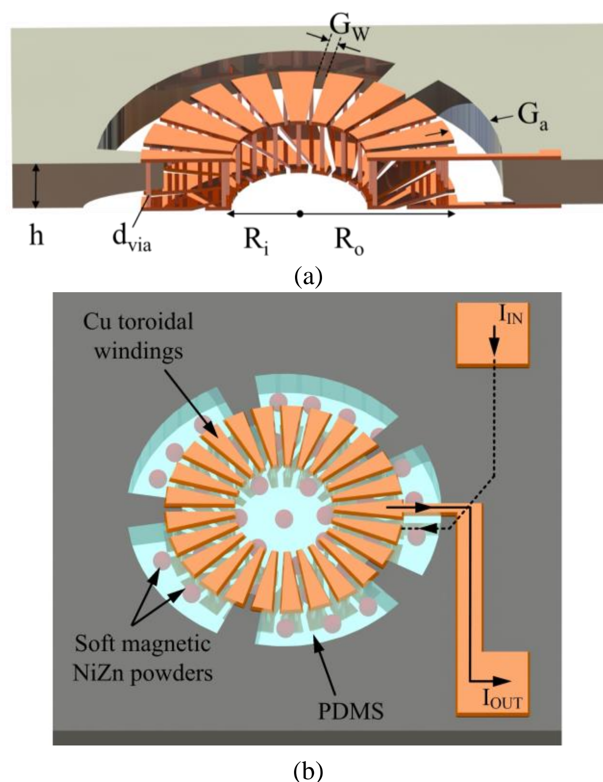

Fig. 1. Designs of the TSV toroidal inductors. (a) A cross-sectional view of a TSV air-core toroidal inductor with a hollow winding structure. The magnetic core consists of 17-μm-diameter soft magnetic NiZn powders mixed in a non-conducting polymer PDMS. The arrows illustrate the direction of the input current (I_{IN}) and output current (I_{OUT}).

0885-8993 (c) 2018 IEEE. Personal use is permitted, but republication/redistribution requires IEEE permission. See http://www.ieee.org/publications_standards/publications/rights/index.html for more information.

This article has been accepted for publication in a future issue of this journal, but has not been fully edited. Content may change prior to final publication. Citation information: DOI 10.1109/TPEL.2018.2847439, IEEE Transactions on Power Electronics

TABLE I
DIMENSIONS OF 3D TSV TOROIDAL INDUCTORS

Parameter	Description	Value	Unit
N	Number of turns	25	turns
R_i	Toroidal inner radius	600	µm
R_o	Toroidal outer radius	1200	µm
h	Inductor height	280	µm
t_{Cu}	Copper slab thickness	50	µm
d_{via}	TSV diameter	50	µm
G_w	Winding gap	90	µm
G_a	Air gap between windings and Si substrate	400	µm

The TSV air-core toroidal inductor is fabricated by a novel MEMS fabrication process reported in [34]. The developed process is based on MEMS fabrication technologies with the focus on CMOS compatibility, scalability, and flexibility. The process consists of three stages: (i) creating TSVs by deep reactive ion etching (DRIE), (ii) electroplating of copper (Cu) and wet-etching of Cu, (iii) Si-core isotropic etching using an inductively coupled plasma (ICP) silicon etching tool to create hollow TSV air-core toroidal inductor. The process has been developed to have low processing temperature of below 200 ^{o}C, thus enabling heterogeneous integration of inductors on CMOS wafers.

Further, a composite magnetic core is filled into the hollow core of the TSV air-core toroidal inductor for making an isotropic toroidal core. The composite core consists of a polymer matrix material and soft-ferrite magnetic powders. The polymer must be a non-conducting material with a low dielectric constant and a high resistivity to minimize parasitic capacitance and eddy-current losses. The soft ferrite powders must have low coercivity (H_c) for high-frequency operations, high resistivity (ρ) for low eddy-current losses, and the powder diameter has to be smaller than the inductor winding gap of 90 µm. A PDMS elastomer (Sylgard Rc 184, Dow Corning, USA) and FP350 (PPtechnology, USA) - fully-sintered soft ferrite NiZn powders are selected as the matrix polymer and the magnetic powders, respectively.

The fabrication process is described in Fig. 2 and animated in the Supplementary Video V1. A mixture of PDMS and FP350 NiZn ferrite powders are prepared and casted into a stainless-steel mold. The stainless-steel mold has two parts: a flat bottom plate and a top plate with a 6 x 6 mm, 300-µm-deep cavity. Two parts are attached together to create the mold in which the FP350-PDMS composite is printed (step 2, Fig. 2b). A planarization step is done to get the desired composite thickness of 300µm (step 3, Fig. 2c). An air-core toroidal inductor is immerged slowly into the mold until the top windings are covered. The sample is cured at 75 ^{o}C for 3 hours on a hot plate. The magnetic-core inductor is obtained after releasing from the mold (step 6, Fig. 2f). Fig. 2g shows a cross-sectional micrograph of the fabricated TSV magnetic-core inductors scanned by an X-ray inspection system

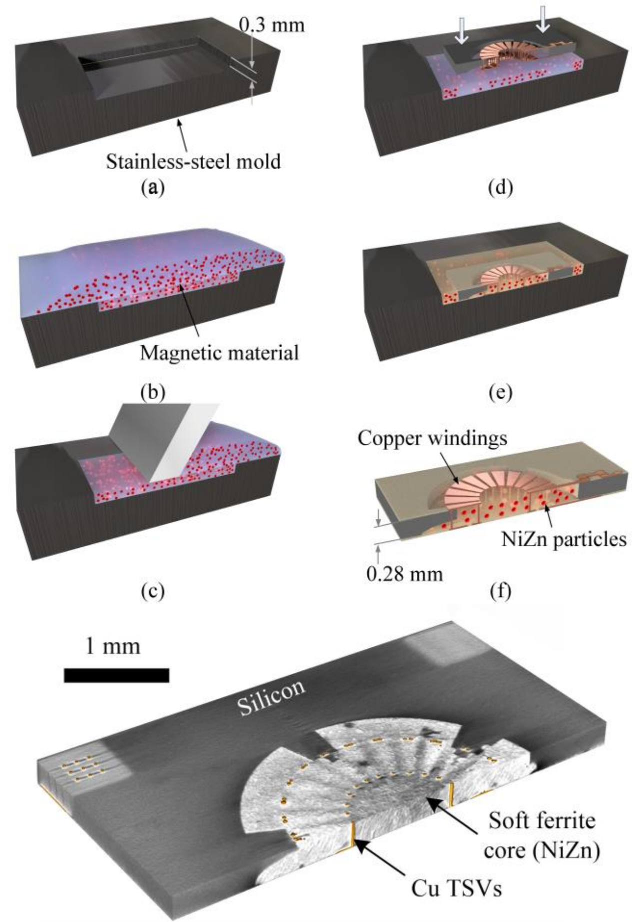

Fig. 2. A manual casting process for magnetic core fabrication. (a) Step 1: a stainless-steel mold with a 0.3-mm-deep, 6 x 6 mm cavity, (b) Step 2: casting of the composite material into the mold, (c) Step 3: a planarization step is done to get a uniform composite layer with a thickness of 0.3 mm, which is designed to be slightly thicker than the inductor thickness of 280 µm to avoid overfilling of the core material over the copper windings. (d) Step 4: immerging of the air-core inductor into the composite layer, (e) Step 5: the core is cured at 75 ^{o}C for 3 hours, (f) Step 6: the inductor is released from the mold. (g) A cross-sectional micrograph of a fabricated TSV magnetic-core toroidal inductor scanned by an X-ray inspection system XD7600NT (Nordson DAGE Corp., UK).

XD7600NT (Nordson DAGE Corp., UK). It is clearly shown that the magnetic core is fully filled without air-voids. In addition, it is noticed that the magnetic material covers the top and bottom windings thus confining the out-of-plan one-turn flux to further minimize the EMI issue.

The important parameters in the casting process are (i) a high-concentration core for a high inductance density, (ii) a homogeneous core with uniformly distributed magnetic powders for a good isolation between the powders, and (iii) a void-free filling without air gaps. In case of distributed air gaps, these will reduce the effective core volume thus reducing the effective permeability (μ_{eff}). In addition, they can create thermal instability due to the thermal expansion generated by the cycled temperature during operation. The casting process is optimized towards these objectives by varying the powder content (C_{FP350}). A high C_{FP350} increases the possibility of forming air gaps. Six inductors were fabricated with the C_{FP350} varies from 63 to 88 weight percent

0885-8993 (c) 2018 IEEE. Personal use is permitted, but republication/redistribution requires IEEE permission. See http://www.ieee.org/publications_standards/publications/rights/index.html for more information.

This article has been accepted for publication in a future issue of this journal, but has not been fully edited. Content may change prior to final publication. Citation information: DOI 10.1109/TPEL.2018.2847439, IEEE Transactions on Power Electronics

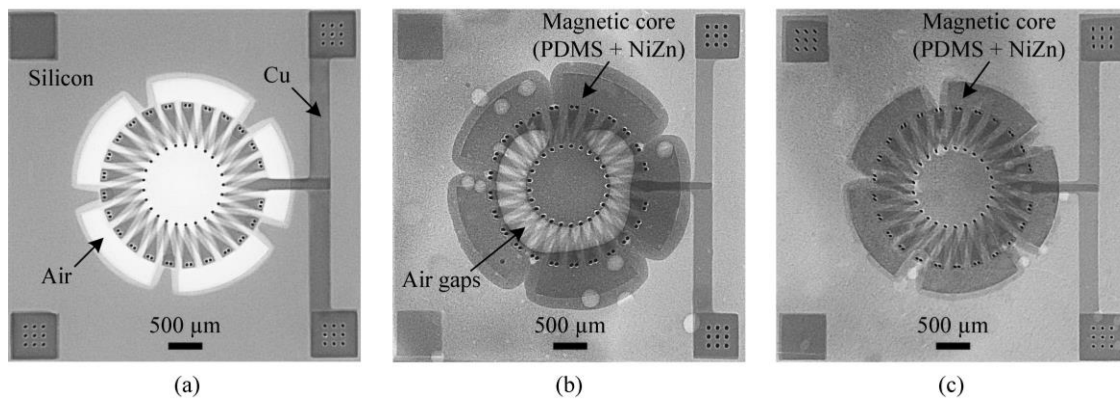

Fig. 3. X-ray micrographs of the fabricated TSV inductors. (a) A 25-turn, 280-μm-thick TSV air-core toroidal inductor. TSV magnetic-core inductors with the soft content C_{FP350} = (b) 88 wt% and (c) 84 wt%. The micrographs were captured by an X-ray inspection system XD7600NT.

(wt%). The results are described in Table II and Fig. 3. At C_{FP350} = 88 wt%, big air avoids were observed as shown in Fig. 3b. The maximum C_{FP350} is 84 wt% for a void-free core as shown in Fig. 3c. Other factors are the curing temperature and curing pressure. A curing temperature was optimized at 75 °C.

The uniformity of the core depends on the size of the magnetic powders which must be smaller than the winding gap of 90 μm. Due to the limiting winding gap, it is required to perform a grinding step [35] for bigger powders or to use finer powders e.g. sub-micron or nanoscale powders [36]–[38]. The inductors made of finer powders will have higher packaging factors thus achieving higher inductance. The proposed process has an advantage in the flexibility to implement different magnetic materials and matrix polymers for other applications e.g. thermal conductive polymers for better thermal dissipation. The proposed fabrication process was made on individual inductor dies but it can be scaled to the wafer-level processing by using a well-established screen-printing technique.

TABLE II
OPTIMIZATION OF CORE CONCENTRATION

No.	FP350 (g)	PDMS (g)	Weight percent (wt%)	Effective μ_r	Fabrication results
1	1	0.5	63	2.3	Fully filled
2	1.5	0.5	71	2.4	Fully filled
3	2	0.5	77	2.5	Fully filled
4	2.5	0.5	81	2.7	Fully filled
5	3	0.5	83	3.0	Fully filled
6	3.8	0.5	88	-	Big air gaps

III. ELECTRICAL CHARACTERIZATION

A. Small Signal Measurement

The TSV air-core and magnetic-core toroidal inductors were electrically characterized using a precision impedance analyzer and vector network analyzer (VNA). The two-port scattering-parameters were measured on a E5071C VNA (0.3 MHz – 20 GHz, Agilent, USA) with 500-μm-pitch ground-signal (GS) probes connected to two terminals of the inductors as shown in Fig. 4c. The measured S-matrix was then converted to the Z-matrix which is used to extract the inductor's equivalent elements i.e. resistance and inductance. The bias measurements were done by using a HP4285 LCR meter and a current source HP42841.

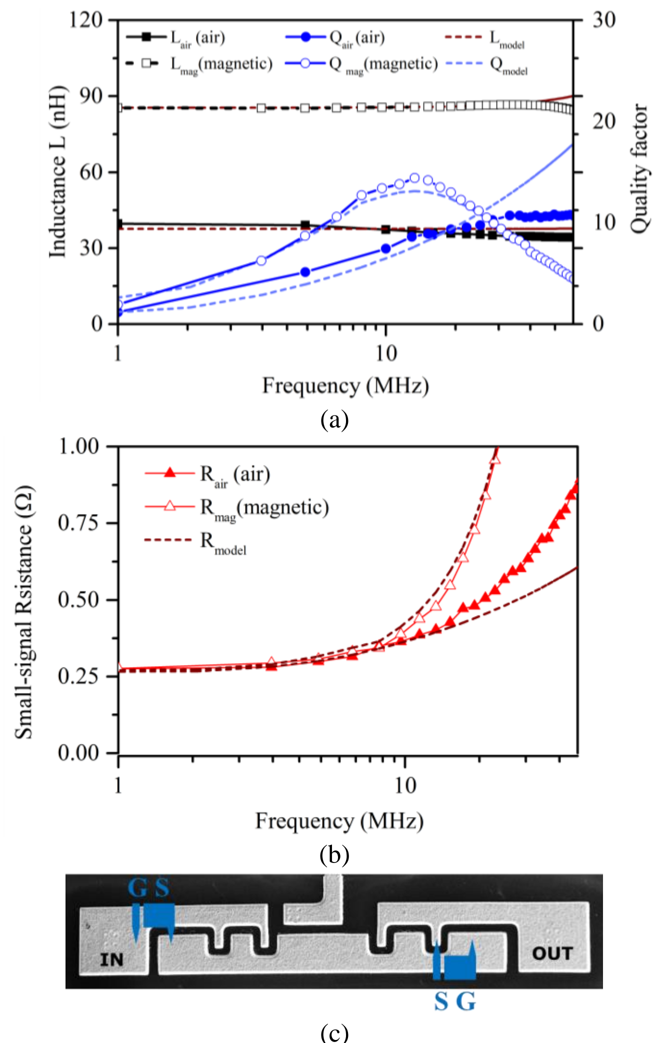

Fig. 4. Small signal measurement and the modeling results of the TSV inductors. (a) Measured inductance of the air-core (L_{air}) and magnetic-core (L_{mag}) TSV inductors and the quality factor of the air-core (Q_{air}) and the magnetic-core (Q_{mag}) TSV inductors. The magnetic -core inductor has a higher peak Q of 14.3 at 12.5 MHz compared to the peak Q of 10.7 at 47 MHz. (b) The measured resistance of the TSV air-core (R_{air}) and magnetic-core (R_{mag}) inductors. The discontinuous lines show the calculation results. (c) An illustration of GS probe on the inductor measurement pads.

Fig. 4 presents the small-signal measurement results of the air-core and magnetic-core TSV toroidal inductors. The

0885-8993 (c) 2018 IEEE. Personal use is permitted, but republication/redistribution requires IEEE permission. See http://www.ieee.org/publications_standards/publications/rights/index.html for more information.

This article has been accepted for publication in a future issue of this journal, but has not been fully edited. Content may change prior to final publication. Citation information: DOI 10.1109/TPEL.2018.2847439, IEEE Transactions on Power Electronics

inductances measured at 1 MHz of the air-core and magnetic-core inductor are 38.2 nH and 86.0 nH, respectively. The calculated inductances using equation (1), are 37.5 nH (air core) and 85.2 nH (magnetic core). Several models for the TSV air-core toroidal inductor are presented in [15], [39]–[41]. A parasitic capacitance model is presented in [40]. The air-core inductance is calculated by eq (1) [40]–[41] with two terms created by an N-turn poloidal current and a single-turn toroidal current, respectively. From 1 to 50 MHz, this model has less than 6.7 % error compared to the measured air-core inductance. The inductance of the TSV magnetic-core toroidal inductor (L_{mag}) is calculated using a relative permeability μ_r =2.4 which is measured by a high-frequency permeameter (PMM-9G1; Ryowa Electronics Co., Ltd., Japan). It is assumed that in the frequency range below 50 MHz, the permeability is frequency-independent.

In Fig. 4a, L decreases slightly with frequency resulting in a slight inductance drop of 4 % at frequencies above 40 MHz. On the other hand, the modelled inductance, which is calculated as the imaginary part of the inductor impedance, increases slightly at the frequency above 40 MHz due to a resonant effect with the measured resonant frequency of 142 MHz. The inductance model for L_{mag} has less than 5.5 % error for the TSV magnetic-core toroidal inductor:

$$L = \mu_r \left[\frac{N^2 h \mu_o}{2\pi} \ln\left(\frac{R_o}{R_i}\right) + \frac{R_o + R_i}{2} \mu_o \left[\ln\left(8 \cdot \frac{R_o + R_i}{R_o - R_i}\right) - 2 \right] \right] \quad (1)$$

where N is the number of turns, h is the inductor height, μ_r is the relative permeability of the core material, R_i and R_o is the inner and outer radius of the TSV toroidal inductor.

Fig. 4a shows that the TSV magnetic-core inductor has a peak Q of 14.3 measured at 12.5 MHz as compared to a peak Q of 10.3 at 47 MHz of the air-core inductor. The increased Q for the magnetic core device is due to the higher inductance and lower eddy current losses in the core material at lower frequencies. On increasing frequencies, the eddy current losses in core increase, reducing the inductance and hence the Q-factor. The inductances measured at 1 MHz of the air-core and magnetic-core inductor are 38.2 nH and 86.0 nH, respectively. Fig. 4b shows the measured and calculated AC resistance (R_{small}) of the TSV air-core and magnetic-core inductors. In this model, it is assumed that the current in the TSVs, top and bottom conductors flows in a skin depth facing the high-field inner region of the toroidal core. The TSV air-core inductor has a resistance of 0.26 Ω at 1 MHz and 0.40 Ω at 12.5 MHz. The calculated resistances are 0.25 Ω and 0.38 Ω at 1 MHz and 12.5 MHz, respectively. For the air-core, the model has an error less than 10 % for frequencies up to 25 MHz. The magnetic-core inductor has a higher resistance with 0.27 Ω at 1 MHz and 0.49 Ω at 13 MHz. The small-signal resistance (R_{small}) is modelled with a winding resistance and an equivalent eddy-current-loss resistance. The winding resistance includes TSVs resistance (R_{via}) and slab resistance (R_{slab}) which are calculated by eq (2) [40] and (3), respectively. The trapezoidal wet-etched profile of the top and bottom windings is accounted in eq (3).

$$R_{Via} = \frac{N\rho h}{2\delta(d_{via} - \delta)}\left(\frac{1}{n_i} + \frac{1}{n_o}\right) \quad (2)$$

$$R_{slab_top} = R_{slab_bot} = N\rho \int_0^l \frac{1}{\delta(f)[2\pi(R_i + x)/N - G_W - 2\delta(f)\, d_e/t_{Cu}]} dx \quad (3)$$

where n_i and n_o are the number of the inner and outer TSVs. ρ is the conductivity of the winding material and $\delta = \sqrt{1/\pi f \mu \sigma}$ is the skin depth where f is frequency, μ is copper permeability ($4\pi 10^{-7}$ H/m), and σ is copper conductivity. h is the wafer thickness and d_{via} = 50 μm is the diameter of the TSVs. d_e is the undercut due to Cu wet etch. The top and bottom slab resistances are calculated using the same eq (3) by replacing the slab length (l) by the top slab length (l_{top}) and the bottom slab length (l_{bot}). l_{top} and l_{bot} are calculated by the eqs. (4) and (5), respectively. G_w = 90 μm is the winding gap.

$$l_{top} = R_o - R_i \quad (4)$$

$$l_{bot} = \sqrt{(R_o - d)^2 + (R_i + d)^2 - 2(R_o - d)(R_i + d)\mathrm{Cos}\left(\frac{2\pi}{N}\right)} + 2d \quad (5)$$

It is noted that the Q model is less accurate at frequencies above 20 MHz with more than 11 % error. This is because the modelled resistance is lower than the measured resistance. The resistance model does not account for the proximity effect between the winding slabs and TSVs. An additional contribution to the resistance is a high current density at the connections between TSVs and the perpendicular winding slabs. This effect is not considered in the resistance model.

Fig. 5a shows the measured L_{mag}, R_{mag}, and Q_{mag} of the TSV magnetic-core inductors fabricated with a core concentration (C_{FP350}) from 63 wt% to 84 wt%. The measurements were operated at 12.5 MHz. As expected, L_{mag} increases from 86 nH to 112 nH for C_{FP350} from 63 wt% to 84 wt%. R_{mag} increases with higher C_{FP350} due to an increased eddy-current loss in larger soft-ferrite volumes. This results in a decrease of Q_{mag} from 14.3 to 11.5. Even though adding the magnetic core improves the Q factor by 30 % compared to that of the air-core inductor, the peak Q still decreases with an increasing C_{FP350}. Adding more core material introduces more core eddy-current losses in the device which has a higher frequency dependency than copper eddy current losses. In addition, because the winding resistance is altered by the strong magnetic field generated in the magnetic core, adding more core material will affect the current density and hence the winding resistance.

Furthermore, the fabricated TSV magnetic-core inductors were characterized under a DC bias current (I_{DC}) from 0 to 1.2 A as shown in Fig. 5b. All tested inductors showed a similar inductance drop of 14.1 % (at I_{DC} = 1.2 A) from its initial inductance (at I_{DC} = 0 A). This drop is due to the saturation response of the soft magnetic materials to the applied field, hence the effective core volume reduces gradually. This reduction results in a lower effective permeability of the core thus reducing the inductance. As the bias current increases, the

0885-8993 (c) 2018 IEEE. Personal use is permitted, but republication/redistribution requires IEEE permission. See http://www.ieee.org/publications_standards/publications/rights/index.html for more information.

This article has been accepted for publication in a future issue of this journal, but has not been fully edited. Content may change prior to final publication. Citation information: DOI 10.1109/TPEL.2018.2847439, IEEE Transactions on Power Electronics

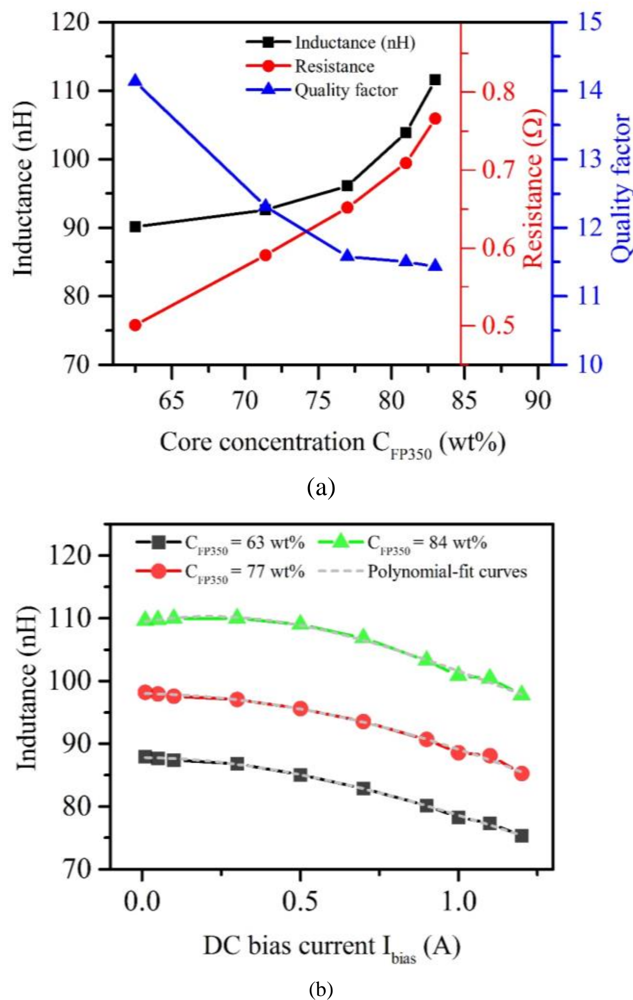

Fig. 5. (a) Measured small-signal L_{mag}, R_{mag}, Q_{mag} as a function of core content C_{FP350} measured at 12.5 MHz. (b) L_{mag} versus bias current (I_{bias}) from 0A to 1.2A. The dashed lines are 3rd-order polynomial fitting curves. A saturation current of 1.6 A is estimated with a 20 % drop of inductance.

core is gradually saturated and thus the inductance decreases. The saturation current (I_{sat}), which is defined by a 20 % drop in inductance, is estimated to be 1.7 A from the extrapolating 3rd-order polynomial fitting curve.

Table III compares the small-signal performance of the fabricated TSV magnetic-core inductors to the prior art of MEMS power inductors. The demonstrated TSV inductors (this study) have a higher Q factor than most of the integrated inductors reported in [9] and in Table III while the inductance and DC resistance are in the same range. The TSV toroidal inductors occupy a footprint of 2.4 x 2.4 mm and a height of 0.28 mm. The proposed inductors are evaluated and compared using a figure of merit (FOM) which is calculated by $FOM = \sqrt{Q_{DC} \cdot Q_{AC}}/V$, where $Q_{DC} = L_{DC}/R_{DC}$, Q_{AC} is the peak small-signal Q, and V is the volume of the fabricated inductor including the substrate thickness for our inductors. The fabricated TSV magnetic-core toroidal inductors have a higher FOM than most of the reported inductors. The FOM employed here includes both the dc and ac performance of the device, which in most cases are inversely dependent. For example devices, which achieve higher inductance densities (solenoid) with increased windings, typically have higher Q_{AC}, but suffer from higher DC resistance. Similarly, devices achieving higher inductance densities with increase magnetic core contribution (stripline) have improved dc losses in comparison to their ac performance. Hence, a FOM where both these factors are considered presents a more realistic comparison between the different devices. One factor still not included in the FOM is the current handling capability of the device, as this data is not widely reported, the authors have chosen to use the FOM metric described above in this study. It is noted that the proposed FOM is useful to evaluate inductor's performance when the contributions between DC and AC performances are equally important, for example zero voltage switching DC-DC buck converter in which inductor carries both DC and AC current.

The performance of the TSV inductors can be improved further by optimizing the winding design, for example smaller winding gaps for higher winding density and larger and denser parallel TSVs for lower winding resistance. Alternative advanced magnetic materials e.g. iron-based nanocrystalline materials [36]–[38] with high saturation and high permeability can be used to enhance the inductance and power density. The magnetic materials have to be pre-sintered to avoid a high-temperature sintering process which is incompatible with CMOS fabrication technologies.

However, small-signal measurements are not sufficient to evaluate the magnetic-core inductor due to the different loss mechanisms in the core, including hysteresis loss and anomalous loss which only appear at large ac currents. Characterization and testing of the magnetic-core inductors in large-signal condition (i.e. large amplitude AC signal or in power converter) is discussed in the next section.

TABLE III
SMALL-SIGNAL PERFORMANCE OF THE TSV MAGNETIC-CORE TOROIDAL INDUCTOR COMPARED TO THE PRIOR WORKS

Study	INDUCTOR	Core	L (nH)	Q_{max} @ f (MHz)	R_{DC} (Ω)	I_{sat} (A)	Footprint (mm^2)	Height (mm)	Figure of Merit (FOM) $\sqrt{Q_{DC} \cdot Q_{AC}}/V$
This study	**In-Si 3D toroid**	**NiZn + PDMS**	**85**	**14.3 @ 12.5**	**0.23**	**1.6**	**5.6**	**0.28**	**46.36**
	In-Si 3D toroid	**NiZn + PDMS**	**112**	**11.5 @ 12.5**	**0.265**	**1.6**	**5.6**	**0.28**	**44.46**
UF [35]	In-Si 2D spiral	NiZn + PDMS	390	10 @ 6	0.140	-	9	0.83	22.34
UF [24]	In-Si 3D toroid	NiZn + PDMS	160	10.5 @ 14	0.265	-	169	0.32	1.47
HKUST [25]	In-Si 3D toroid	MnZn + PDMS	43.6	16.2 @ 65	0.28	-	2.9	-	-
Gatech [14]	In-Si 3D toroid	Air	60	17.5 @ 70	0.191	-	36	0.6	3.43
Gatech [26]	In-Si 3D toroid	CoNiFe	1000	18 @ 1	0.7	-	100	1	1.60

UF: University of Florida, USA; HKUST: Hong Kong University of Science and Technology, Hong Kong; Gatech: Georgia Institute of Technology, USA.

0885-8993 (c) 2018 IEEE. Personal use is permitted, but republication/redistribution requires IEEE permission. See http://www.ieee.org/publications_standards/publications/rights/index.html for more information.

This article has been accepted for publication in a future issue of this journal, but has not been fully edited. Content may change prior to final publication. Citation information: DOI 10.1109/TPEL.2018.2847439, IEEE Transactions on Power Electronics

B. Large Signal Measurement

The large-signal losses of the TSV magnetic-core inductor were measured in the frequency range from 10 to 15 MHz. The measurement setup consists of two blocks: the signal generation system and the measurement system. The signal generation system generates a sinusoidal excitation current with a high-amplitude, high-frequency AC current along with a DC bias current. The AC current is generated by a signal generator E8257D (250 KHz – 20 GHz, Agilent, USA) and then amplified by an RF-amplifier model 25A250A (10 kHz - 250 MHz, Amplifier Research, USA). A DC bias current is generated by a bench top power supply 72-10480 (3A, TENMA, Japan). The voltage and current across the inductor are sensed by 1.5 GHz active probes (Tektronix, USA) and recorded by a mixed domain oscilloscope MDO3104 (Tektronix, USA). The details of the measurement technique including current sensing and compensation are reported in [42], [43].

Fig. 6 shows the large-signal testing results of a 63-wt% TSV magnetic-core toroidal inductor. The inductance and total resistance (R_{total}) were measured with a DC bias current from 0 to 1.6 A and a 12.5 MHz, 0.2 A AC current. The inductance drops 17 % at bias current of 1.6 A giving an estimated saturation current of 1.7 A. R_{total} increases from 1 to 2 Ω as the frequency increase from 10 to 15 MHz. R_{total} includes all core losses including the hysteresis loss and the anomalous loss which are neglected in small-signal measurement due to smaller excitation AC currents. The measured R_{total} is shown in Fig. 6. It is noted that R_{total} drops from 1.48 Ω to 1.35 Ω with an increased bias current from 0 to 1.6 A. This can be explained by the fact that when some portion of the core enters saturation, the effective core volume reduces. The saturated core volume does not contribute to the inductance but also does not add to the losses. Hence, increasing the DC current leads to a lower inductance and a lower AC core resistance.

Fig. 7 show the core loss separation from the large-signal testing of 63-wt% TSV magnetic-core inductor. The total loss (P_{total}) consists of four losses including eddy-current core loss and winding loss ($P_e + P_w$),hysteresis loss (P_h), and anomalous loss (P_a). P_{total} is calculated from the large-signal resistance by $P_{total} = R_{total} \cdot I_{acrms}^2$. It is interesting to note, as the test frequency is increased from 10 MHz to15 MHz, the contribution of $P_e + P_w$ decreases from 49% to 35 % of the total loss. Assuming that the magnetic core does not significantly alter the current density in the copper windings, the winding resistance is the same for the TSV air-core and magnetic-core toroidal inductors. Hence, by subtracting the air-core resistance, the increased resistance is due to the added magnetic core. This increased resistance results in an additional core loss which is considered as the eddy-current loss (P_e). P_e contributes an average proportion of 13.6 ± 0.15 % to P_{total} at the frequency from 10 to 15 MHz. This is because the magnetic powders have high resistivity and they are isolated with high-resistivity PDMS.

The core loss is analyzed as follows: The eddy-current loss

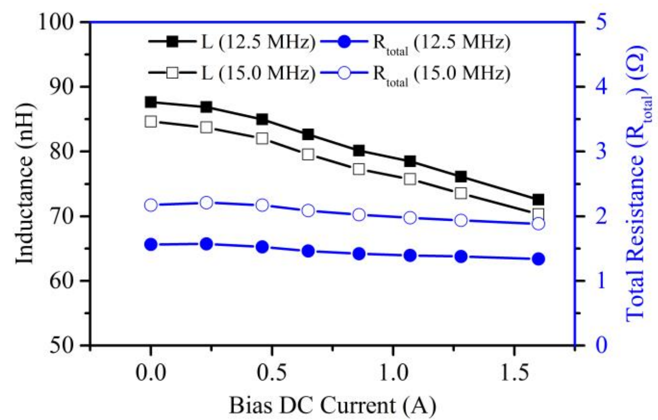

Fig. 6. The large-signal inductance and resistance (R_{total}) of a 63-wt% TSV magnetic-core inductor with a 200-mA peak-to-peak AC current and DC currents (0 – 1.6 A).

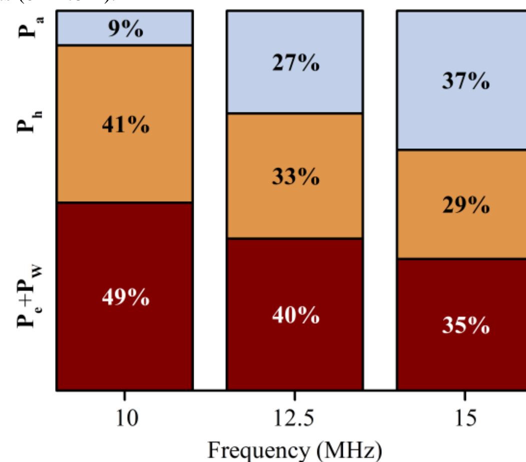

Fig. 7. Core loss separation of a 63 wt% TSV magnetic-core toroidal inductor based on large-signal measurements. The winding loss and eddy-current loss ($P_w + P_e$) from small signal measurement, the hysteresis loss (P_h), and the anomalous loss (P_a) are shown in the percentage measured from 10 to 15 MHz

in powder-core inductor is empirically modelled by the model developed by Skarrie [44]. The measured small-signal resistance as the experimental data to determine the eddy-current loss coefficient. A similar method was reported in [45]. Specifically, the small-signal core loss is determined by subtracting the total small-signal resistance (R_{mag}) to the winding resistance (R_W) assuming that the added magnetic-core material does not alter the current distribution in the copper windings. This assumption has been verified by Han et al. [46] for a low-permeability magnetic-core inductor ($\mu_r < 4$), therefore, for our inductors which have a μ_r from 2.2 to 3.0 the reported approach of subtracting winding resistance is applicable. The hysteresis loss is modelled using (6) [47], and the anomalous loss, which is the subtraction of the total loss to the other losses, is calculated by $P_a = P_{total} - P_e - P_w - P_h$.

$$P_h = 4 f B_{ac}{}^2 \frac{H_c}{B_{sat}} \tag{6}$$

where f is the excitation frequency, B_{sat} is the saturation magnetic flux density, B_{ac} is the applied AC flux density, and H_c is the coercivity.

0885-8993 (c) 2018 IEEE. Personal use is permitted, but republication/redistribution requires IEEE permission. See http://www.ieee.org/publications_standards/publications/rights/index.html for more information.

This article has been accepted for publication in a future issue of this journal, but has not been fully edited. Content may change prior to final publication. Citation information: DOI 10.1109/TPEL.2018.2847439, IEEE Transactions on Power Electronics

The proportion of the hysteresis loss is therefore corresponding to 41 % and 29 % the total core loss at 10 and 15 MHz. The anomalous loss, which is the subtraction of the total loss to the other losses, is calculated by $P_a = P_{total} - P_e - P_w - P_h$. It is noted that the anomalous loss contributes 9% and 37% of the total loss at 10 MHz and 15 MHz, respectively. The loss mechanism of the anomalous loss is often explained as excess eddy-currents which appear along the ferrite grain boundaries when subjected to fast switching, large ac fields. This is different to traditional eddy currents which are a macroscopic loss, primarily frequency-dependent phenomena and appear within the material to oppose flow of flux. The anomalous losses are dependent both on frequency and amplitude of applied ac fields.

From the calculated losses, equivalent resistances for the core loss can be calculated to build an equivalent model of the TSV magnetic-core toroidal inductor (Fig. 8) which can be used for inductor design.

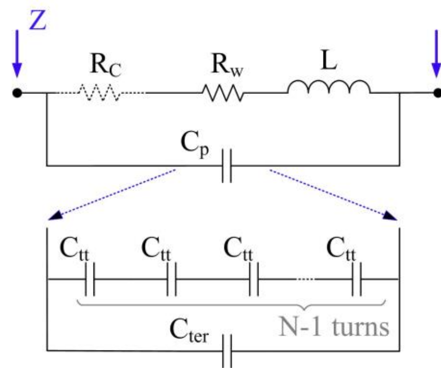

Fig. 8. An equivalent model of the complex impedance (Z) of the TSV air-core toroidal inductor with a winding resistance (R_w), an ideal inductance (L), and a winding capacitance (C_p). An equivalent core resistance (R_c) representing the total core loss is added to model the TSV magnetic-core toroidal inductor. C_p includes a terminal capacitance (C_{ter}) between inductor input and output and N – 1 turn-to-turn capacitance (C_{tt}) connected in serial.

IV. 12 MHz Buck Converter

A high frequency soft-switching buck converter was designed and implemented using an 85-nH TSV magnetic-core toroidal inductor and gallium nitride (GaN) field effect transistors (FETs). A schematic of the converter's power stage is shown in Fig. 9a. The converter consists of two EPC8004 40 V GaN FETs (Q_{HS} and Q_{LS}) driven by a LM5113 high speed gate driver, a TSV magnetic-core toroidal inductor (L), input capacitors (C_{IN}) and output capacitors (C_{OUT}). An assembled converter is shown in Fig. 9b in which the TSV magnetic-core toroidal inductor under test is connected to the converter board via a test board using low-resistance copper wires. The contribution from the connection wires is included in the converter simulation with an additional inductance of 20 nH. The test board is used to measure the inductor's small-signal performance and to estimate the power loss in the inductor under test. The power stage is driven by a tunable pulse width modulator with an adjustable dead time capability. A summary of the designed voltage regulator components is shown in Table IV.

The detailed operation of such zero-voltage switching (ZVS) converter using an air-core spiral inductor is reported in [48]. The converter along with the TSV inductor is simulated

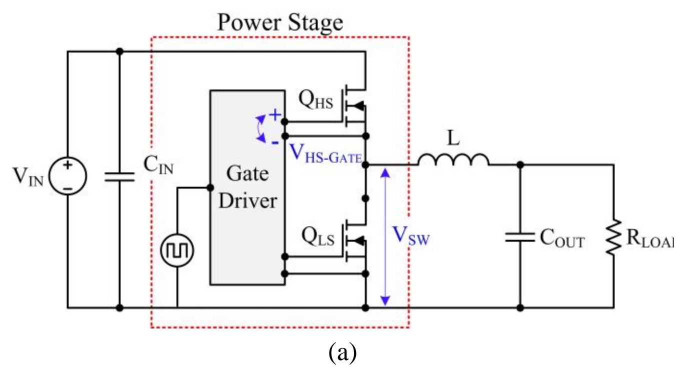

(a)

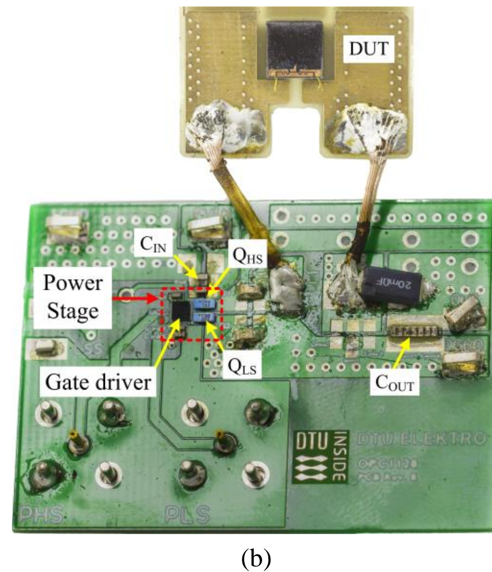

(b)

Fig. 9: (a) A schematic and (b) An optical image of a buck converter using two 40-V GaN FETs and a TSV magnetic-core inductor under test (DUT).

TABLE IV
Testing Specification for a Buck Converter

Parameter	Value	Description
V_{IN}	12 V	Input Voltage
V_{OUT}	3.3 – 5 V	Output Voltage
I_{OUT}	0 – 0.5 A	Output Current
f_{SW}	12 MHz	Switching Frequency
L	85 nH	Inductance

using LT-spice. The simulation model for the inductor was built based on the small-signal and large-signal measurements to account for the winding loss and the core losses. Fig. 10 presents the simulated and measured waveforms. Fig. 10a shows the simulated waveforms of the high-side gate voltage with 3.3 V output voltage. The switching voltage (V_{SW}) waveforms verify that the converter is operating in ZVS mode. Fig. 10b shows the simulated inductor current which consists of a 0.5 A DC current and a 0.84 A RMS AC current. The measured waveform at the switching node is shown in Fig. 10c which indicates that the converter operates in ZVS when the FETs are turning ON. It is also noted from the measured waveform that the converter is partially soft switching due to the probe capacitance loading effect. When a probe is used to measure the switching node voltage (V_{SW}), an additional capacitance from the probe (C_{probe}) is added to the circuit in parallel to the C_{oss}, as the result, it takes more time to

0885-8993 (c) 2018 IEEE. Personal use is permitted, but republication/redistribution requires IEEE permission. See http://www.ieee.org/publications_standards/publications/rights/index.html for more information.

This article has been accepted for publication in a future issue of this journal, but has not been fully edited. Content may change prior to final publication. Citation information: DOI 10.1109/TPEL.2018.2847439, IEEE Transactions on Power Electronics

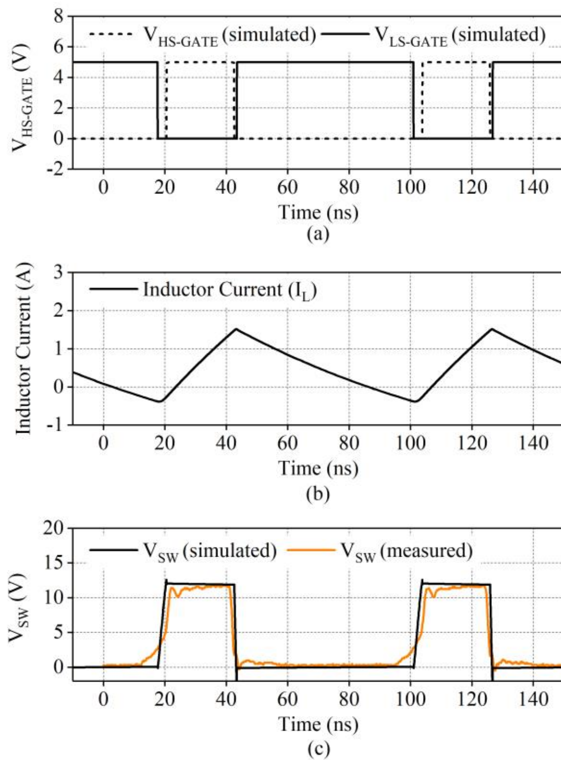

Fig. 10: (a) Simulated waveform of the high-side gate voltage ($V_{HS\text{-}GATE}$), (b) Simulated waveform of the inductor current, (c) Simulated and measured waveforms of the switching voltage (V_{SW}).

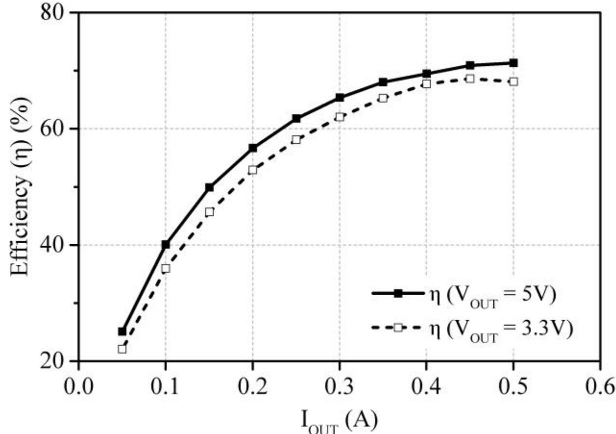

Fig. 11: The measured efficiency (η) with the output current (I_{OUT}) from 0 to 0.5 A. The output voltage (V_{OUT}) is 3.3 V and 5 V. A peak η of 71.6 % was achieved at V_{OUT} = 5 V.

discharge the capacitance (C_{oss} + C_{probe}) by the negative inductor current (I_L) before the FETs turn on. Fig. 11 presents the efficiency (η) as a function of the output current (I_{out}) from 0 to 0.5 A for two output voltages of 3.3 V and 5 V. The converter achieves a peak efficiency of 71.6 % at V_{out} = 5 V and P_{out} = 2.4 W.

The power loss of the TSV magnetic-core toroidal inductor in the converter is determined by the thermal measurement method [49] via DC power loss. The power loss is 0.52 W and 0.79 W for V_{out} of 3.3V and 5 V, respectively. Fig. 12 shows the thermal images of the inductor under the AC power loss in the converter (Fig. 12 a, b) and the DC power loss (Fig. 12 c, d). It is noted that in the magnetic-core inductor, the heat is dissipated more uniformly through the magnetic core confirming the advantage of the magnetic core for better heat

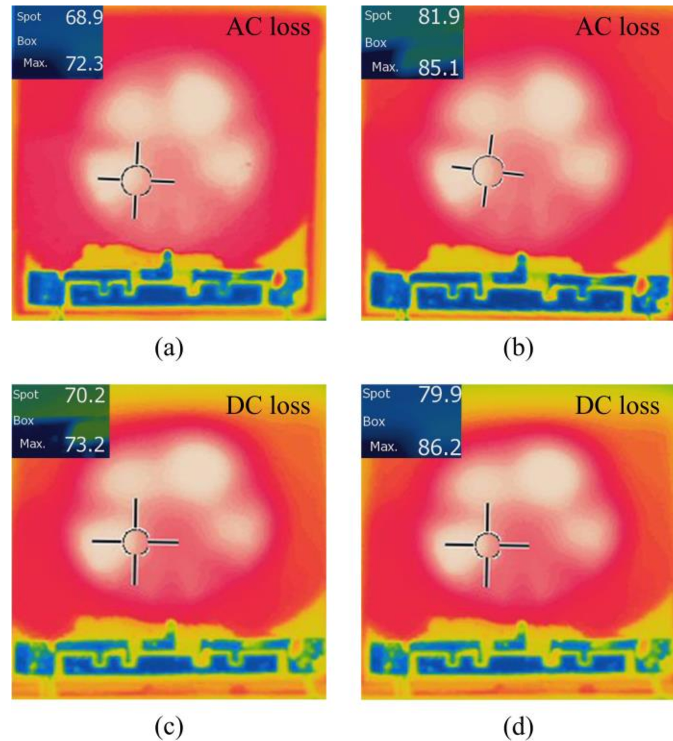

Fig. 12: Thermal image of a TSV magnetic-core inductor in the converter at I_{OUT} = 0.5 A with the output voltage of (a) V_{out} = 3.3 V, (b) V_{out} = 5.0 V. A thermal image of the inductor under a DC power loss of (c) 0.52 W (V_{DC} = 0.56 V, I_{DC} = 1.11 A) and (d) 0.79 W (V_{DC} = 0.65 V, I_{DC} = 1.23 A). The DC power loss in the inductor is 0.52 W and 0.79 W for V_{out} of 3.3 V and 5V, respectively.

transfer. The thermal performance could be further improved by replacing PDMS by a thermal epoxy e.g. EPO-TEK® 921-FL (Epotek, USA has thermal conductivity = 1.1 W/mK, and high resistivity > 6. 10^{11} Ωm).

V. Conclusion

A high-Q TSV magnetic-core toroidal inductor for high frequency (10 – 20 MHz) power conversions has been reported. The TSV magnetic-core toroidal inductors were modelled, fabricated, characterized and tested in a high-frequency converter. The fabricated TSV NiZn-core toroidal inductors have a peak Q factor of 14.3 and an inductance of 85 – 112 nH. A selected inductor was used to implement a 12-MHz ZVS buck converter which achieved a peak efficiency of 71.6 % and successfully delivered 2.4 W to the output at the input voltage of 12 V and the output voltage of 3.3 V and 5 V. The magnetic core was integrated using a simple casting process with the potential of printing a wide range of microscale magnetic powders for other applications. Furthermore, using TSVs to build the in-Si inductor could enable the fabrication of passive interposers with integrated 3D inductors for PSiP and potentially for PwrSoC integration.

Appendix

The calculation of slab resistance is presented as follows:
Slab width at position x ($W(x)$):

$$W(x) = \frac{2\pi(R_i + x)}{N} - G_w \quad (7)$$

0885-8993 (c) 2018 IEEE. Personal use is permitted, but republication/redistribution requires IEEE permission. See http://www.ieee.org/publications_standards/publications/rights/index.html for more information.

This article has been accepted for publication in a future issue of this journal, but has not been fully edited. Content may change prior to final publication. Citation information: DOI 10.1109/TPEL.2018.2847439, IEEE Transactions on Power Electronics

Cross-sectional area $A(x)$:

$$A(x) = \delta(f)W(x) - \delta(f)^2 \frac{d_e}{t_{Cu}} \quad (8)$$

$$R_{slab} = N\int \frac{\rho}{A(x)}dx = N\int \frac{\rho}{\delta(f)W(x) - \delta(f)^2 \frac{d_e}{t_{Cu}}}dx \quad (9)$$

Resistance of N Cu slab R_{slab}:

$$R_{slab} = N\rho \int_0^l \frac{1}{\delta(f)[2\pi(R_i + x)/N - G_W - 2\delta(f)\, d_e/t_{Cu}]}dx \quad (10)$$

Top slab length l_{top}:

$$l_{top} = R_o - R_i \quad (11)$$

Bottom slab length l_{bot}:

$$l_{bot} = l + 2d = \sqrt{(R_o - d)^2 + (R_i + d)^2 - 2(R_o - d)(R_i + \mathrm{d})\mathrm{Cos}(2\pi/N)} + 2d \quad (12)$$

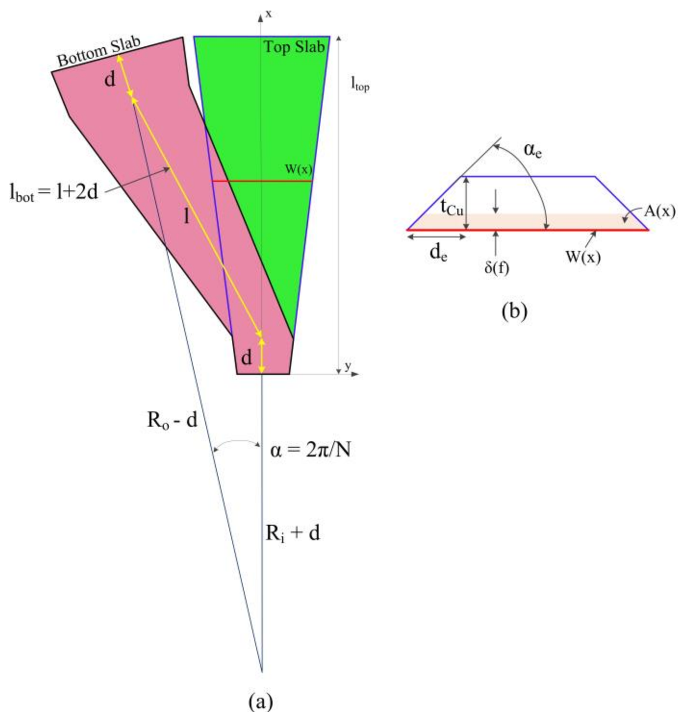

Fig. 13. Illustration for calculation of slab resistance. (a) Illustrations of top and bottom slab, (b) A cross-sectional view of the trapezoidal slab.

ACKNOWLEDGEMENT

This work has been conducted at the National Center for Micro- and Nanofabrication (DTU Danchip), DTU Electrical Engineering, and Tyndall National Institute, Ireland. This project is a part of TinyPower project which is funded by Innovation Fund, Denmark (No. 67-2014-1). The authors would like to acknowledge funding from Science Foundation Ireland through their Starting Investigator (15/SIRG/3569) and Investigators Programme (15/IA/3180).

REFERENCES

[1] D. Bandyopadhyay and J. Sen, "Internet of things: Applications and challenges in technology and standardization," in Wirel. Pers. Commun., 2011, vol. 58, no. 1, pp. 49–69.
[2] D. Miorandi, S. Sicari, F. De Pellegrini, and I. Chlamtac, "Internet of things: Vision, applications and research challenges," Ad Hoc Networks, vol. 10, no. 7. pp. 1497–1516, 2012.
[3] S. Li, L. Da Xu, and S. Zhao, "The internet of things: a survey," Inf. Syst. Front., vol. 17, no. 2, pp. 243–259, 2015.
[4] G. Sauerländer, D. Hente, H. Radermacher, E. Waffenschmidt, and J. Jacobs, "Driver electronics for LEDs," in Conf. Rec. IEEE 41st IAS Annu. Meet., 2006, vol. 5, pp. 2621–2626.
[5] S. C. O'Mathuna, "PwrSiP power supply in package power system in package," in 2016 Int. Symp. 3D Power Electron. Integr. Manuf., 2016, pp. 1–21.
[6] F. Waldron, R. Foley, J. Slowey, A. N. Alderman, B. C. Narveson, and S. C. Ó Mathúna, "Technology roadmapping for power supply in package (PSiP) and power supply on chip (PwrSoC)," IEEE Trans. Power Electron., vol. 28, no. 9, pp. 4137–4145, 2013.
[7] M. Araghchini et al., "A Technology Overview of the PowerChip Development Program," IEEE Trans. Power Electron., vol. 28, no. 9, pp. 4182–4201, 2013.
[8] S. C. Ó. Mathúna, T. O'Donnell, N. Wang, and K. Rinne, "Magnetics on silicon: An enabling technology for power supply on chip," IEEE Trans. Power Electron., vol. 20, no. 3, pp. 585–592, 2005.
[9] C. Ó. Mathúna, N. Wang, S. Kulkarni, and S. Roy, "Review of integrated magnetics for Power Supply on Chip (PwrSoC)," IEEE Trans. Power Electron., vol. 27, no. 11, pp. 4799–4816, 2012.
[10] D. Disney and Z. J. Shen, "Review of silicon power semiconductor technologies for power supply on chip and power supply in package applications," IEEE Trans. Power Electron., vol. 28, no. 9, pp. 4168–4181, 2013.
[11] V. Ermolov et al., "Microreplicated RF toroidal inductor," IEEE Trans. Microw. Theory Tech., vol. 52, no. 1 I, pp. 29–37, 2004.
[12] T. M. Liakopoulos and C. Science, "3-D Microfabricated Toroidal Planar Inductors with Different Magnetic Core Schemes for MEMS and Power Electronic Applications," IEEE Trans. Magn., vol. 35, no. 5, pp. 1–3, 1999.
[13] J. Kim, F. Herrault, X. Yu, M. Kim, R. H. Shafer, and M. G. Allen, "Microfabrication of air core power inductors with metal-encapsulated polymer vias," J. Micromech. Microeng., vol. 23, no. 3, p. 35006, Mar. 2013.
[14] X. Yu, M. Kim, F. Herrault, C.-H. Ji, J. Kim, and M. G. Allen, "Silicon-Embedding Approaches to 3-D Toroidal Inductor Fabrication," J. Microelectromech. Syst., vol. 22, no. 3, pp. 580–588, Jun. 2013.
[15] P. Kamby, A. Knott, and M. A. E. Andersen, "Printed circuit board integrated toroidal radio frequency inductors," in 37th Annu. Conf. IEEE Ind. Electron. Soc. - IECON 2011, 2012, pp. 680–684.
[16] C. H. Ahn and M. G. Allen, "A planar micromachined spiral inductor for integrated magnetic microactuator applications," J. Micromech. Microeng., vol. 3, no. 2, pp. 37–44, 1999.
[17] J. Wibben and R. Harjani, "A High-Efficiency DC – DC Converter Using 2 nH Integrated Inductors," IEEE J. Solid-State Circuits, vol. 43, no. 4, pp. 844–854, 2008.
[18] C. R. Sullivan and S. R. Sanders, "Design of microfabricated transformers and inductors for high-frequency power conversion," IEEE Trans. Power Electron., vol. 11, pp. 228–238, 1996.
[19] R. Meere, S. Member, T. O. Donnell, H. J. Bergveld, and N. Wang, "Analysis of Microinductor Performance in a 20–100 MHz DC/DC Converter," IEEE Trans. Power Electron., vol. 24, no. 9, pp. 2212–2218, 2009.
[20] X. Gao et al., "Fabrication of Ultralow-Profile Micromachined Inductor With Magnetic Core Material," IEEE Trans. Magn., vol. 41, no. 12, pp. 4397–4400, 2005.
[21] Y. Yoon, J. Park, and M. G. Allen, "Polymer-Core Conductor Approaches for RF MEMS," J. Microelectromech. Syst., vol. 14, no. 5, pp. 886–894, 2005.
[22] L. Gu and X. Li, "High-Q solenoid inductors with a CMOS-compatible concave-suspending MEMS process," J. Microelectromech. Syst., vol. 16, no. 5, pp. 1162–1172, 2007.
[23] X. Yu, M. Kim, F. Herrault, C. Ji, J. Kim, and M. G. Allen, "Silicon-embedded 3D toroidal air-core inductor with through-wafer interconnect for on-chip integration," in Micro Electro Mech. Syst., 2012, no. February, pp. 325–328.
[24] J. Li, K. D. T. Ngo, G. Lu, and H. Xie, "Wafer-level fabrication of high-power-density MEMS passives based on silicon molding technique," Int. Conf. Integr. Power Electron. Syst., vol. 9, pp. 5–9, 2012.
[25] X. Fang, S. Member, R. Wu, L. Peng, S. Member, and J. K. O. Sin, "A

0885-8993 (c) 2018 IEEE. Personal use is permitted, but republication/redistribution requires IEEE permission. See http://www.ieee.org/publications_standards/publications/rights/index.html for more information.

This article has been accepted for publication in a future issue of this journal, but has not been fully edited. Content may change prior to final publication. Citation information: DOI 10.1109/TPEL.2018.2847439, IEEE Transactions on Power Electronics

Novel Silicon-Embedded Toroidal Power Inductor With Magnetic Core," IEEE Electron Device Lett., vol. 34, no. 2, pp. 292–294, 2013.

[26] J. Kim, J.-K. Kim, M. Kim, F. Herrault, and M. G. Allen, "Microfabrication of toroidal inductors integrated with nanolaminated ferromagnetic metallic cores," J. Micromech. Microeng., vol. 23, no. 11, p. 114006, Nov. 2013.

[27] C. R. Sullivan, "Integrating magnetics for on-chip power: Challenges and opportunities," Proc. Cust. Integr. Circuits Conf., no. Cicc, pp. 291–298, 2009.

[28] J. Li, V. F. Tseng, Z. Xiao, and H. Xie, "A High-Q In-Silicon Power Inductor Designed for Wafer-Level Integration of Compact," IEEE Trans. Power Electron., vol. 32, no. 5, pp. 3858–3867, 2017.

[29] R. Meere, T. O'Donnell, S. Kulkarni, S. Roy, and S. C. O'Mathuna, "Magnetic-Core and Air-Core Inductors on Silicon: A Performance Comparison up to 100 MHz," IEEE Trans. Magn., vol. 47, no. 10, pp. 4429–4432, Oct. 2011.

[30] J. Qiu and C. R. Sullivan, "Radial-Anisotropy Nanogranular Thin-Film Magnetic Material for Toroidal Inductors," in Appl. Power Electron. Conf. Expo., 2012, pp. 491–497.

[31] J. Y. Park and M. G. Allen, "Development of magnetic materials and processing techniques applicable to integrated micromagnetic devices," J. Micromech. Microeng., vol. 8, no. 4, pp. 307–316, 1999.

[32] I. Kowase, "A planar inductor using Mn-Zn ferrite/polyimide composite thick film for low-voltage and large-current dc-dc converter," IEEE Trans. Magn., vol. 41, no. 10, pp. 3991–3993, 2005.

[33] F. C. Lee and Q. Li, "High-frequency integrated point-of-load converters: Overview," IEEE Transactions on Power Electronics, vol. 28, no. 9. pp. 4127–4136, 2013.

[34] H. T. Le, I. Mizushima, P. T. Tang, Z. Ouyang, F. Jensen, and A. Han, "Fabrication of 3D Air-core MEMS Inductors for High Frequency Power Electronic Applications," Microsystems Nanoeng., vol. 3, 2017.

[35] M. Wang, J. Li, K. D. T. Ngo, and H. Xie, "A surface-mountable microfabricated power inductor in silicon for ultracompact power supplies," IEEE Trans. Power Electron., vol. 26, no. 5, pp. 1310–1315, 2011.

[36] H. P. System, B. Zhao, S. Member, Q. Song, W. Liu, and Y. Sun, "Overview of Dual-Active-Bridge Isolated Bidirectional DC – DC Converter for," IEEE Trans. Power Electron., vol. 29, no. 8, pp. 4091–4106, 2014.

[37] W. Shen, F. F. Wang, S. Member, D. Boroyevich, and C. W. Tipton, "Loss Characterization and Calculation of Nanocrystalline Cores for High-Frequency Magnetics Applications," IEEE Trans. Power Electron., vol. 23, no. 1, pp. 475–484, 2008.

[38] W. Shen, F. Wang, S. Member, D. Boroyevich, and C. W. T. Iv, "High-Density Nanocrystalline Core Transformer for High-Power High-Frequency Resonant Converter," IEEE Trans. Ind. Appl., vol. 44, no. 1, pp. 213–222, 2008.

[39] J. Pejtersen and A. Knott, "Design and measurement of planar toroidal transformers for very high frequency power applications," Conf. Proc. - 2012 IEEE 7th Int. Power Electron. Motion Control Conf. - ECCE Asia, IPEMC 2012, vol. 1, pp. 688–692, 2012.

[40] G. Zulauf, W. Liang, and J. Rivas-davila, "A Unified Model for High-Power , Air-Core Toroidal PCB Inductors," in IEEE Work. Control Model. Power Electron., 2017.

[41] C. R. Sullivan, S. Prabhakaran, S. Lu, C. R. Sullivan, W. Li, and S. Prabhakaran, "Design and Fabrication of Low-Loss Toroidal Air-Core Inductors," in IEEE Power Electron. Spec. Conf., 2007, pp. 1754–1759.

[42] C. Fernandez, Z. Pavlovi, S. Kulkarni, P. Mccloskey, and C. O. Mathúna, "High Frequency , Single / Dual phases , Large AC / DC signal power characterization for two phase on-silicon coupled inductors," in IEEE Appl. Power Electron. Conf. Expo., 2017, pp. 2488–2493.

[43] C. Fernandez, Z. Pavlovic, S. Kulkarni, P. McCloskey, and C. O. Mathuna, "Novel High Frequency Electrical Characterization technique for Magnetic Passive Devices," IEEE J. Emerg. Sel. Top. Power Electron., vol. 6777, no. c, pp. 1–1, 2018.

[44] H. Skarrie, "Design of Powder Core Inductors," Lund University, 2001.

[45] N. Waveforms, C. R. Sullivan, J. Li, T. Abdallah, and C. R. Sullivan, "Improved Calculation of Core Loss with Nonsinusoidal Waveforms," in IEEE Ind. Appl. Soc. Annu. Meet., 2001, pp. 2203–2210.

[46] Y. Han, G. Cheung, A. Li, C. R. Sullivan, and D. J. Perreault, "Evaluation of magnetic materials for very high frequency power applications," IEEE Trans. Power Electron., vol. 27, no. 1, pp. 425–435, 2012.

[47] S. Kulkarni et al., "Low Loss Magnetic Thin Films for Off-Line Power Conversion," IEEE Trans. Magn., vol. 50, no. 4, pp. 3–6, 2014.

[48] Y. Nour, Z. Ouyang, A. Knott, and I. H. H. Jørgensen, "Design and Implementation of High Frequency Buck Converter Using Multi-Layer PCB Inductor," 42nd Annu. Conf. IEEE Ind. Electron. Soc., pp. 1313–1317, 2016.

[49] H. T. Le, Y. Nour, A. Han, F. Jensen, Z. Ouyang, and A. Knott, "Microfabricated Air-core Toroidal Inductor In Very High Frequency Power Converters," IEEE J. Emerg. Sel. Top. Power Electron., vol. PP, pp. 1–1, 2018.

Hoa Thanh Le (S'15) received the B.Sc. degree in Electronics and Telecommunications from Ho Chi Minh University of Technology, Vietnam, in 2012 and the M:Sc. degree in Microsystem Engineering from University College of Southeast Norway, Norway, in 2014. He received the Ph.D. degree in Micro and Nanotechnology from Technical University of Denmark in 2018. He is currently a Post-Doctoral Researcher with the Department of Micro- and Nanotechnology (DTU Nanotech), Technical University of Denmark, Denmark. His research interests include micro- and nanofabrication, passive components, high frequency magnetics, and catalytic reactors.

Yasser Nour (S'07, M'17) received the B.Sc. and M.Sc. degrees in Electrical Engineering from South Valley University, Egypt in 2007 and 2011 respectively. He was a research engineer at Enpirion Inc., a staff engineer at Altera's Egypt Technology Center, and a staff engineer at Symmid Corporation Sdn. Bhd. in Malaysia. He is currently pursuing the PhD in electrical engineering at Technical University of Denmark. His research interests include analog integrated circuits design, integrated power converters, high voltage low power converters, integrated magnetics and passive components.

Zoran Pavlovi´c received the Ph.D. degree in power electronics from the Universidad Politecnica de Madrid, Madrid, Spain, in 2013. He is currently a Post-Doctoral Researcher with the Integrated Magnetics Group, Tyndall National Institute, Cork, Ireland. His research interests include developing high-efficiency microinductors and micro-transformers on silicon for high-frequency dc–dc converters.

Cian Ó Mathúna (M'05–SM'07–F'13) has 30 years' experience in applied research and technology transfer in microelectronics. He is currently the Head of Strategic Programmes, Tyndall National Institute, University College Cork (UCC), Cork, Ireland. He has held technical and executive positions at the National Microelectronics Research Centre, UCC; the Irish Government Programme in Advanced Technology in Power Electronics, PEI Technologies; and Tyndall National Institute, University College Cork. He is a co-author of over 200 publications and has sourced research funding of over €35 million. His current research interests include system integration/miniaturisation of smart sensor systems for the Internet of Things, miniaturisation/integration technologies for energy harvesting/scavenging and power supply-on-chip (PwrSoC). He is the founder of the International Workshop on Power Supply on Chip and a Research Professor with the School of Engineering, UCC. In 2013, Prof. Ó Mathúna was elevated Fellow of IEEE with the citation "for leadership in the development of power supply using micromagnetics on silicon."

0885-8993 (c) 2018 IEEE. Personal use is permitted, but republication/redistribution requires IEEE permission. See http://www.ieee.org/publications_standards/publications/rights/index.html for more information.

This article has been accepted for publication in a future issue of this journal, but has not been fully edited. Content may change prior to final publication. Citation information: DOI 10.1109/TPEL.2018.2847439, IEEE Transactions on Power Electronics

Arnold Knott (M'10) received the Diplom-Ingenieur (FH) degree from the University of Applied Sciences in Deggendorf, Germany, in 2004. From 2004 until 2009 he has been working with Harman/Becker Automotive Systems GmbH in Germany and USA, designing switch-mode audio power amplifiers and power supplies for automotive applications. In 2010 he earned the Ph.D. degree from the Technical University of Denmark, Kongens Lyngby, Denmark working on a research project under the title "Improvement of out-ofband Behaviour in Switch-Mode Amplifiers and Power Supplies by their Modulation Topology". From 2010 to 2013 he was Assistant Professor and since 2013 Associate Professor at the Technical University of Denmark. His interests include switch-mode audio power amplifiers, power supplies, active and passive components, integrated circuit design, acoustics, radio frequency electronics, electromagnetic compatibility and communication systems.

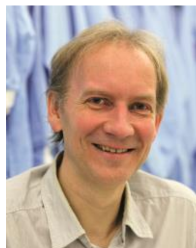

Flemming Jensen received the Ph.D. degree in Physics from the Department of Physics and Astronomy at Aarhus University, Denmark, in 1992. From 1992 until 1997 he worked as a researcher at the newly established cleanroom facility, Microelectronics Center (MIC) – from 2004 renamed DTU Danchip - at the Technical University of Denmark establishing and developing new fabrication technologies in etching and thin film deposition mainly for the silicon based platform. From 1997 he has been an Associate Professor conducting and supporting research projects related to micro- and nanofabrication within various research topics. From 2004 he has been member of the management at DTU Danchip heading the Process Engineering group. In the later years his main focus has been on advanced high density plasma etching techniques for many different material platforms and establishing atomic layer deposition for conformal growth of very thin layers.

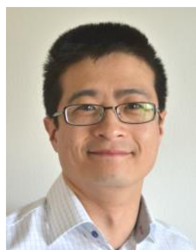

Anpan Han (M' 12) received the B.Sc. and M.Sc. degree in biophysics from the Niels Bohr Institute, University of Copenhagen, Denmark, in 2002. He received the Ph.D. degree in Micro and Nanotechnology from Institute of Microtechnology (now part of EPFL), Université de Neuchâtel, Switzerland in 2006. Currently, he is an assistant professor at Danchip, Technical University of Denmark since 2014. His research is in nanofabrication technology and science, with focus in diamond MEMS, complex MEMS process integration and electron beam lithography.

Santosh Kulkarni (M'12) received the M.Phil. degree in microelectronics engineering and semiconductor physics from the Cavendish Laboratory, University of Cambridge, Cambridge, U.K., and the Ph.D. degree from University College Cork, Cork, U.K. His Ph.D. thesis was on design, simulation, microfabrication and batch-fabrication of vibration-based electromagnetic micropower generators on silicon. He was a Senior Researcher in energy processing with the ICT Group, Microsystems Centre, Tyndall National Institute, Cork. He is involved in power magnetics for buck, offline converters, and voltage regulators. He is currently a Principal Engineer with Dialog Semiconductor, Swindon, U.K. He is also responsible for the development of magnetics technology for passive components in power management circuits. He has published over 55 papers in journals and peer-reviewed conference proceedings, and a book chapter, with an h-index of 15, along with a patent (filed). He developed the power magnetics technology, which has been licensed to large multinational companies.

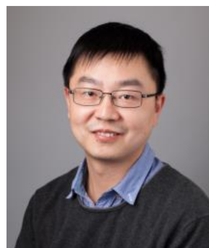

Ziwei Ouyang (S'07, M'11, SM'17) received his PhD degree from Technical University of Denmark (DTU) in 2011. From 2011 to 2013, he was a postdoc researcher at DTU. From 2013 to 2016, he was appointed as an assistant professor at the same department. Since from April 2016, he is an associate professor at DTU. His research areas focus on high-frequency planar magnetics modeling and integration, high-density high-efficiency power converters, PV battery energy storage system, and wireless charging etc.

He is IEEE senior member. He has over 60 high impact IEEE journal and conference publications, co-author on a book chapter on Magnetics for the "Handbook of Power Electronics" and currently he is the holder of 8 international patents. He was a recipient of Young Engineer Award at PCIM-Asia 2014, and received Best Ph.D. Dissertation of the Year Award 2012 in Technical University of Denmark. He received several Best Paper Awards in IEEE sponsored international conferences. He has been invited to give lectures in many universities, enterprises and educational seminars and workshops around the world including USA, Europe and China. He has served as session chair in some IEEE sponsored conferences and reviewer for the IEEE Transactions on power electronics and IEEE Transactions on Industrial Electronics. Currently, he is responsible for the Power Electronics course for both undergraduate and graduate students at DTU, and he also supervised more than 40 students' projects including Postdoc, Ph.D. and Master projects.

0885-8993 (c) 2018 IEEE. Personal use is permitted, but republication/redistribution requires IEEE permission. See http://www.ieee.org/publications_standards/publications/rights/index.html for more information.